Supplementary Information

Mn (II)-hemoporfin-based metal-organic frameworks as a theranostic nanoplatform for MRI-guided sonodynamic therapy

Qin Jiang, [a] Hao Xu, [a] Wen Zhang, [a] Yue Wang, [*b] Jindong Xia, [b] Zhigang Chen [*a]

[a.] *State Key Laboratory for Modification of Chemical Fibers and Polymer Materials, Colleges of Materials Science and Engineering, Donghua University, Shanghai 201620, China.*
[b.] *Department of Radiology, Shanghai Songjiang District Central Hospital, Shanghai 201600, China.*

1. Experimental Section

1.1. Materials

hemoporfin was purchased from Shanghai Xianhui Pharmaceutical; manganese chloride, N, N-dimethylformamide (DMF), methanol, 1,3-diphenylisobenzofuran (DPBF), triethylamine, and anhydrous ethanol were purchased from Sinopharm Chemical Reagent; distearoyl phosphoethanolamine-polyethylene glycol (DSPE-PEG, Mw=5000, 99%) was purchased from Shanghai Yanyi Biotechnology; fetal bovine serum, Roswell Park Memorial Institute-1640 (RPMI-1640), and Dulbecco's modified Eagle's medium (DMEM) were purchased from Gibco; and 2',7'-dichlorofluorescin diacetate (DCFH-DA), 4',6-diamidino-2-phenylindole (DAPI), Calcein-AM, propodium iodide (PI) and phosphate buffer saline (PBS) were purchased from Beyotime Biotechnology.

1.2. Characterization

The morphologies were characterized by a S-4800 scanning electron microscopy (SEM) and a FEI Talos F200S transmission electron microscopy (TEM). The high-resolution TEM images were acquired under an acceleration voltage of 200 kV. The elemental compositions and valency states were analyzed using a Escalab 250Xi X-ray photoelectron spectroscopy (XPS). The absorption spectra were measured by a Shimadzu UV-3600 UV-vis spectrophotometer; Fourier-transform infrared (FT-IR) spectra were obtained by a Shimadzu IRPrestige-21 FT-IR spectroscopy; and

* Corresponding author: E-mail address: zgchen@dhu.edu.cn (Z. Chen); wymyf@163.com (Y. Wang)

fluorescence property were recorded by a JASCO FP-6600 fluorescence spectrophotometer. The absorbance of cells was tested by a ThermoFisher Multiskan MK3 microplate reader. The cells were imaged by an Olympus BX51 fluorescence microscope. The magnetic resonance imaging (MRI) of mice was performed by a UIH uMR770 3.0T clinical MRI system.

1.3. MRI Effect In Vitro

The magnetic resonance imaging capacities of Mn (II)-hemoporfin-PEG and manganese chloride ($MnCl_2$) was examined at different concentrations of Mn^{2+} ions (0, 0.025, 0.05, 0.1, 0.2, and 0.4 mM), using a 0.5T field MR scanner. The longitudinal relaxivity (r_1) values were determined by plotting a standard curve using the concentrations of Mn^{2+} and the corresponding $1/T_1$ relaxation time.

1.4. In Vivo Imaging and Sonodynamic Therapy

Tumor model: Balb/c mice were obtained from Zhejiang Charles River Laboratory Animal Technology Co., Ltd. All animal experiments were performed in accordance with the protocols approved by the Animal Welfare and Research Ethics Committee of Donghua University. The CT26 cell xenograft model was built by subcutaneous injection of about 5×10^6 cells. The calculation of tumor size follows tumor volume = tumor length × tumor width^2 × 0.5.

In vivo imaging: Tumor-xenografted mice were received an intravenous injection of Mn (II)-hemoporfin-PEG (10 mg/kg body weight). At designated time points (0, 2, 4, 8, and 24 h), mice were anesthetized with isoflurane for MRI examination.

In vivo sonodynamic therapy: The mice were randomly divided into four groups (n=4 per group): (1) PBS, (2) PBS with ultrasound irradiation, (3) Mn (II)-hemoporfin-PEG (10 mg/kg body weight), (4) Mn (II)-hemoporfin-PEG (10 mg/kg body weight) with ultrasound irradiation. PBS and Mn (II)-hemoporfin-PEG were intravenously injected into the mice. The tumor areas of groups 2 and 4 were irradiated by ultrasound (1 MHz, 50% duty cycle, 1.75 W/cm^2, 10 min) at 8 h and 24 h after injection. Tumor size and body weight were measured and calculated every 2 days. In addition, tumor size was also recorded by MRI system during treatment process and the maximum

tumor cross-section of image was used to measure tumor volume. On day 12, mice were euthanized, and then, the heart, liver, spleen, lung, kidney, and tumor were taken out and fixed in 4% paraformaldehyde for hematoxylin and eosin staining.

2. Supplementary Figures

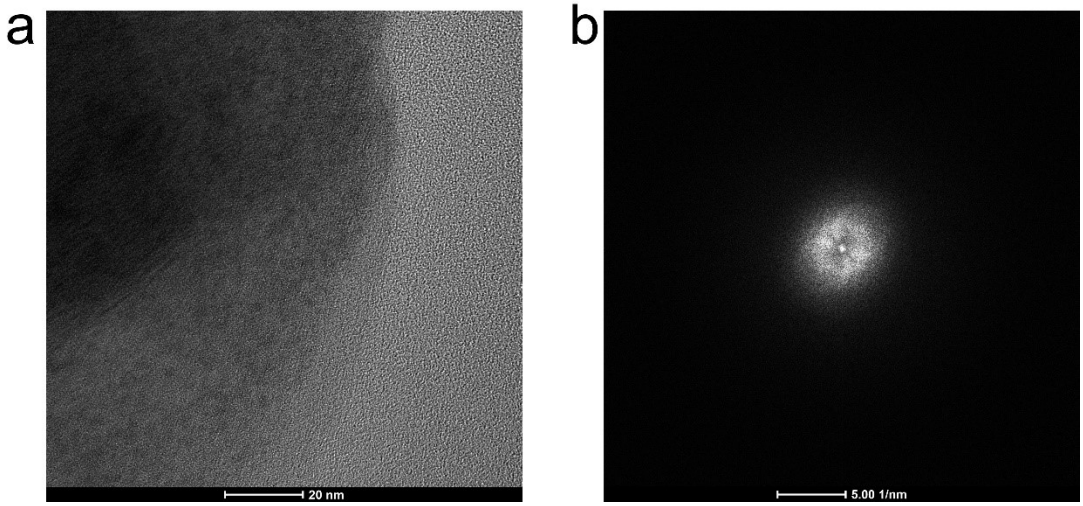

Fig. S1 (a) High magnification TEM image and (b) FFT pattern of Mn (II)-hemoporfin.

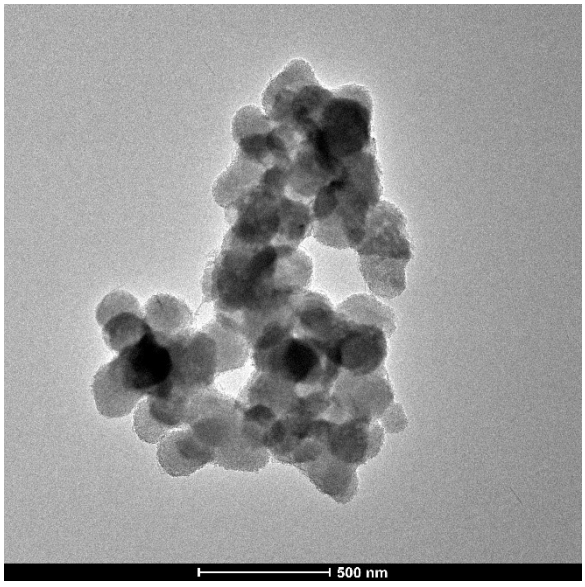

Fig. S2 TEM image of Mn (II)-hemoporfin-PEG.

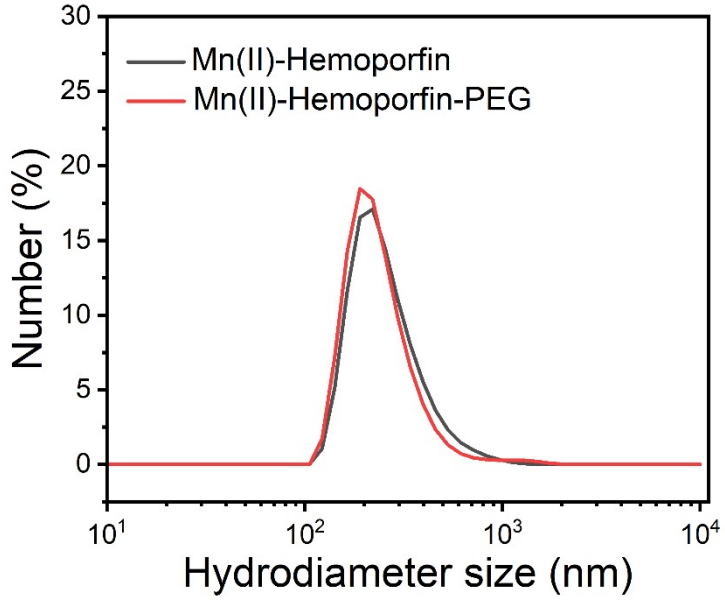

Fig. S3 Hydrodiameter sizes of Mn (II)-hemoporfin-PEG and Mn (II)-hemoporfin.

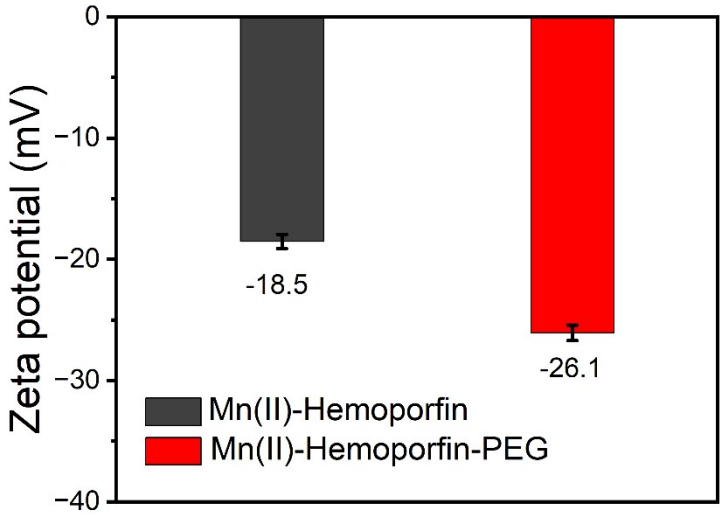

Fig. S4 Zeta potentials of Mn (II)-hemoporfin-PEG and Mn (II)-hemoporfin.

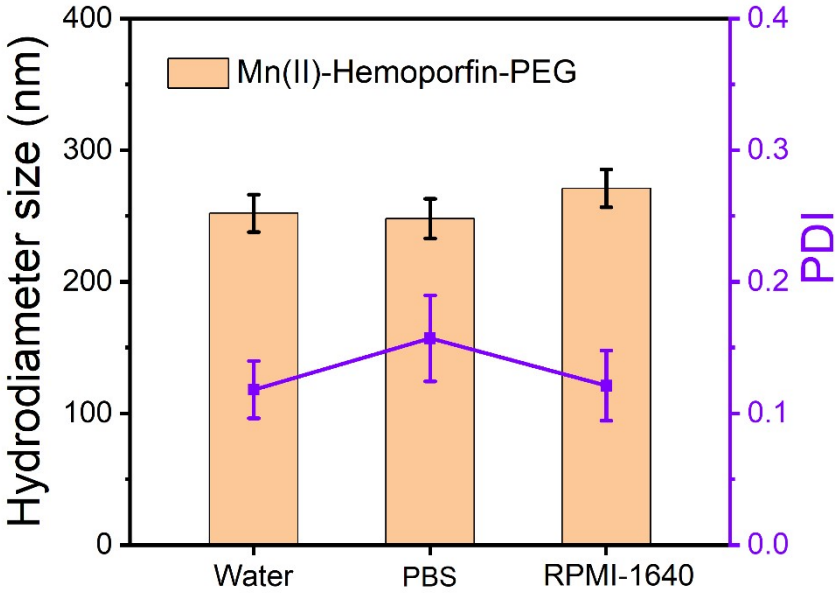

Fig. S5 Hydrodiameter sizes and PDI of Mn (II)-hemoporfin-PEG in water, PBS, and RPMI-1640 with 10% FBS.

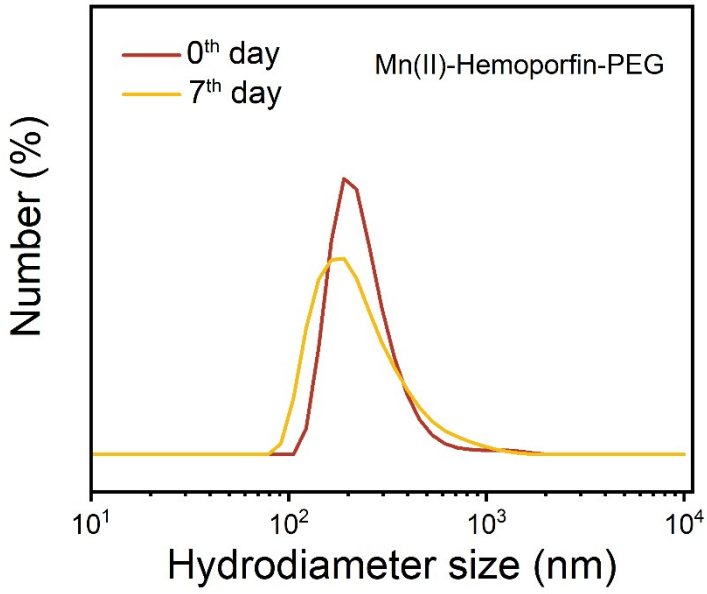

Fig. S6 Hydrodiameter size of Mn (II)-hemoporfin-PEG after 7 days of storage.

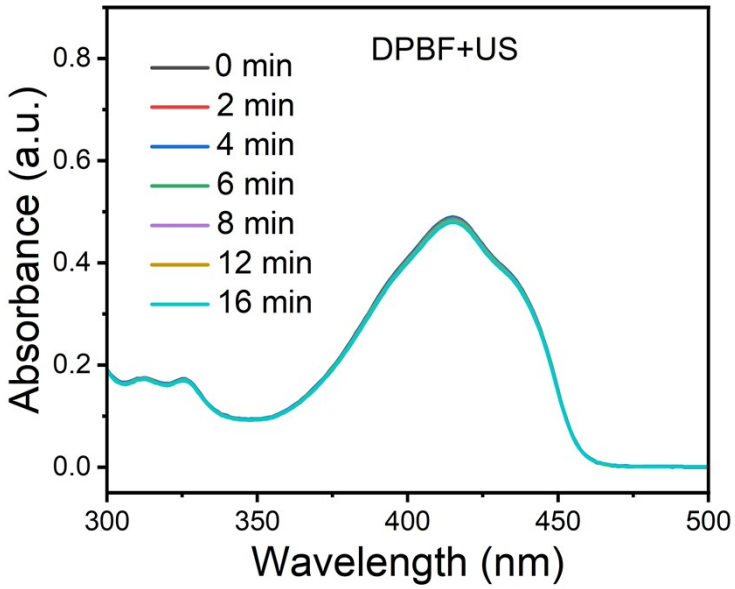

Fig. S7 Absorbance change of DPBF under different times of irradiation.

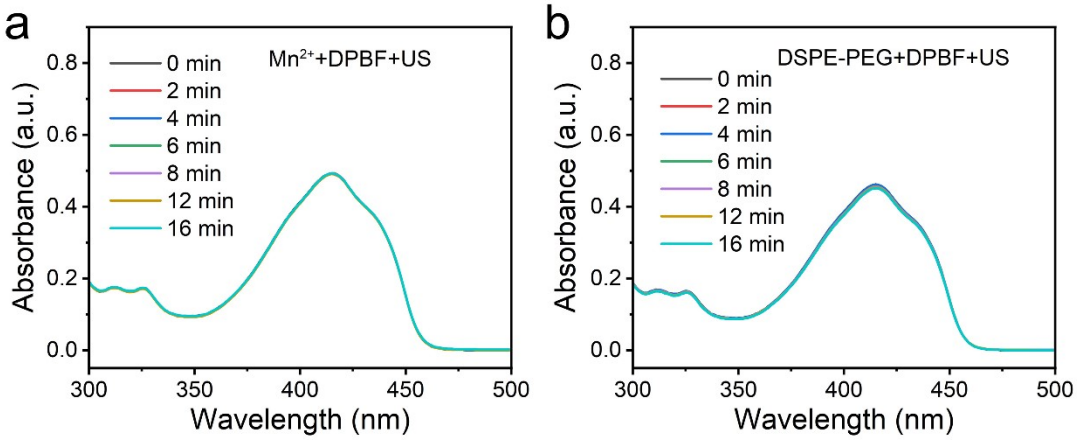

Fig. S8 Absorbance change of DPBF in (a) Mn^{2+} and (b) DSPE-PEG solution under different times of irradiation.

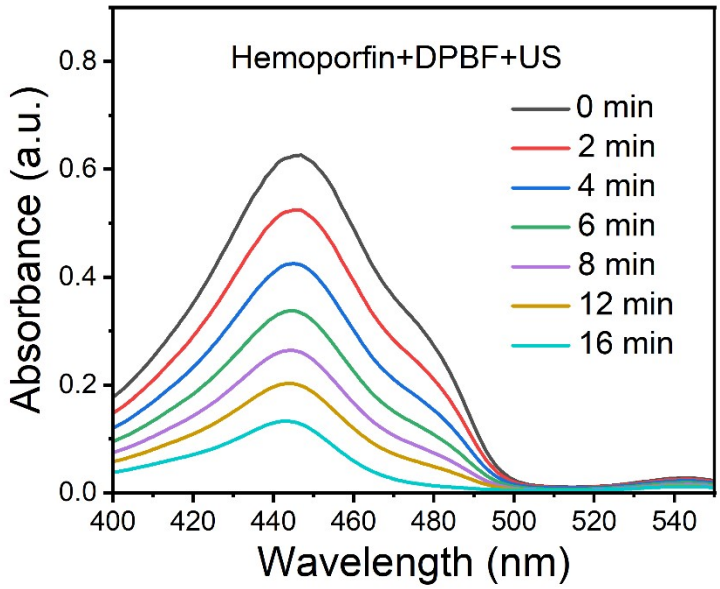

Fig. S9 Absorbance change of DPBF in hemoporfin solution under different times of irradiation.

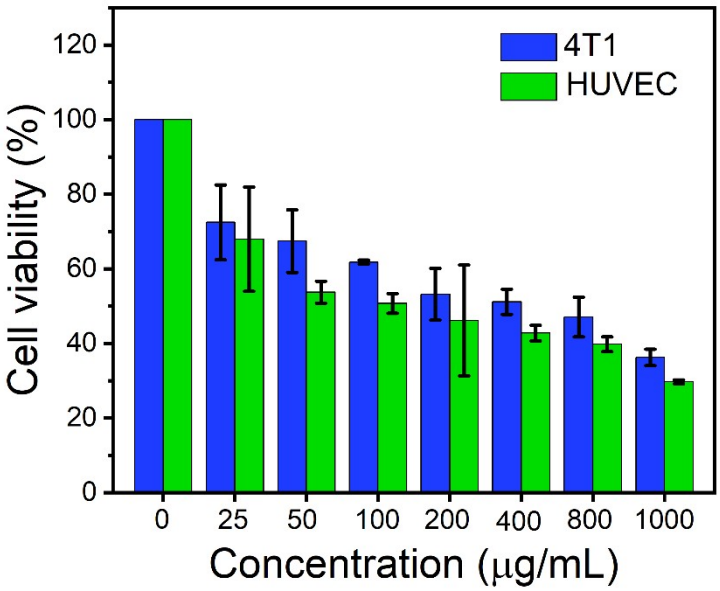

Fig. S10 Cell viability of 4T1 and HUVEC cells after incubated with different concentrations of Mn (II)-hemoporfin-PEG and irradiated with ultrasound for 3 min, respectively.

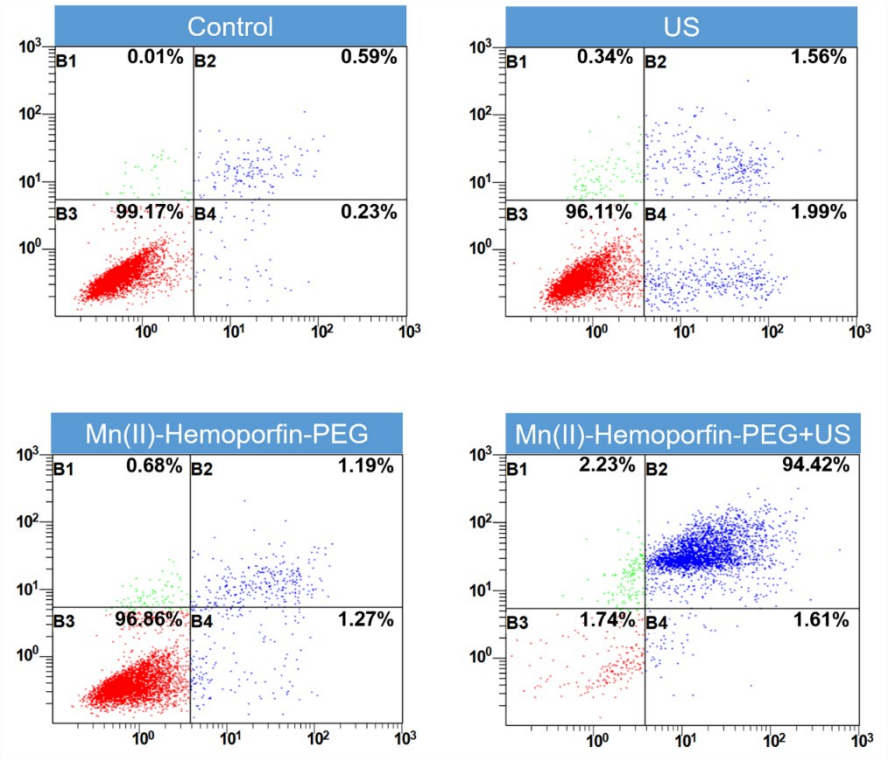

Fig. S11 Flow cytometry analysis of CT26 cells after treatment with different groups.

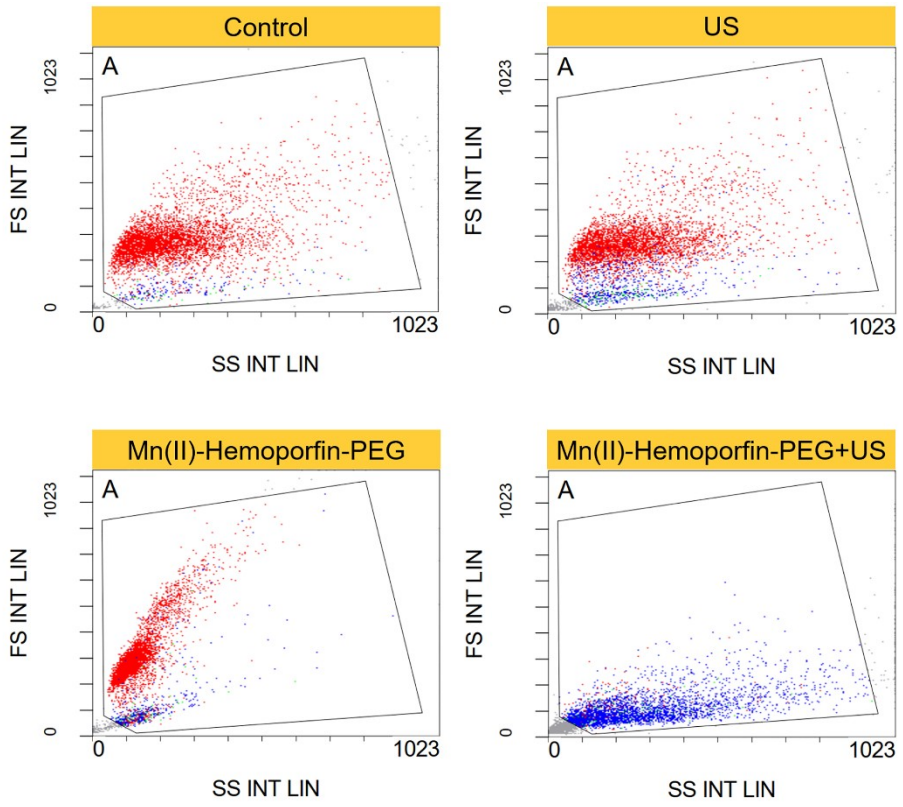

Fig. S12 Flow gating strategies for CT26 cells after treatment with different groups.

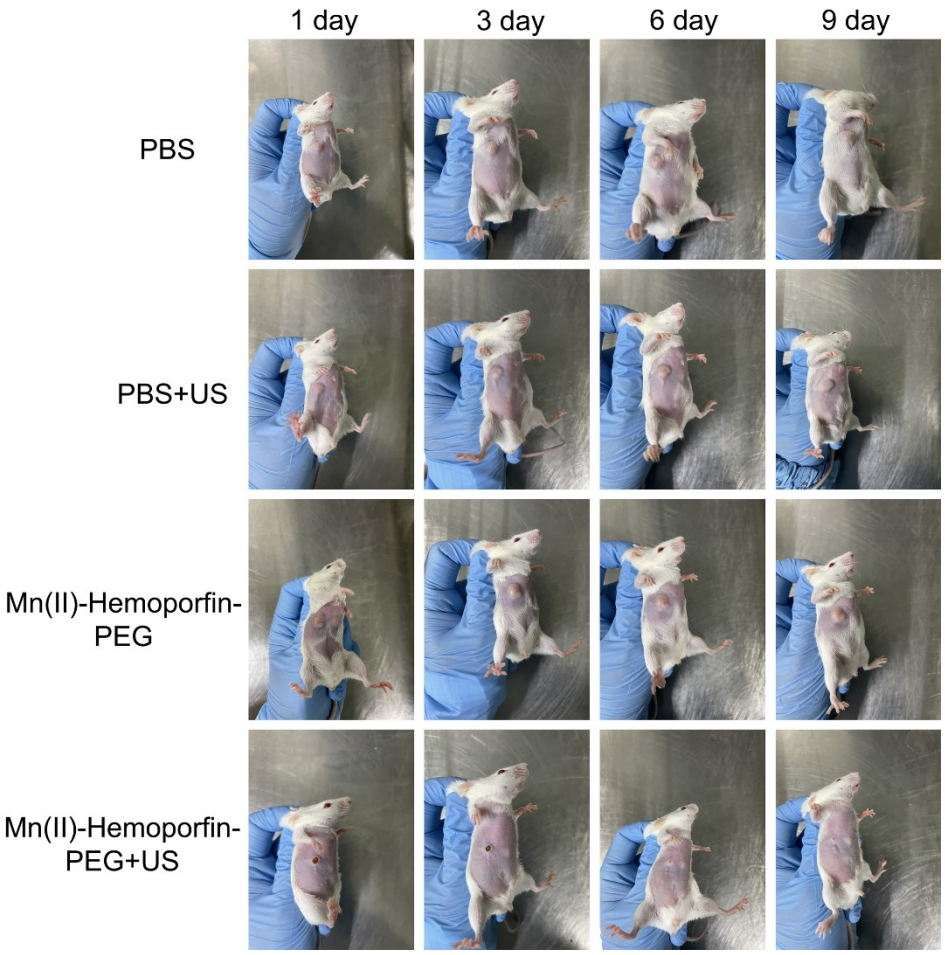

Fig. S13 Representative digital photos of mice from different groups during treatment process.